

Graphene Moiré patterns observed by umklapp double-resonance Raman scattering

A. Righi,¹ S. D. Costa,¹ H. Chacham,¹ C. Fantini,¹ P. Venezuela,² C. Magnuson,³
L. Colombo,⁴ W. S. Bacsa,⁵ R. S. Ruoff,³ and M. A. Pimenta¹

¹*Departamento de Física, Universidade Federal de Minas Gerais, 30123-970, Belo Horizonte, Brazil*

²*Instituto de Física, Universidade Federal Fluminense, Niteroi, Brazil*

³*Department of Mechanical Engineering and the Texas Materials Institute, University of Texas at Austin, 1 University Station C2200, Austin, Texas 78712-0292, USA*

⁴*Texas Instruments Incorporated, 13121 TI Boulevard, MS-365 Dallas, Texas 75243, USA*

⁵*CEMES/CNRS, University of Toulouse, 29 rue Jeanne Marvig, FR-31055 Toulouse, France*

(Received 6 December 2011; published 28 December 2011)

This work reports a Raman study of graphene bilayer samples grown by chemical vapor deposition on a copper foil, using laser lines in the UV range. The Raman spectra show a number of extra peaks, classified in different families, which appear nonuniformly across the Cu surface, in regions with sizes of several μm . We interpret these new extra modes as due to Moiré patterns of twisted layers of graphene, each family of peaks being associated with different twist rotational angles. We theoretically analyze the results, introducing the concept of umklapp double-resonance Raman processes associated with reciprocal lattice vectors of the Moiré pattern supercells.

DOI: [10.1103/PhysRevB.84.241409](https://doi.org/10.1103/PhysRevB.84.241409)

PACS number(s): 68.65.Pq, 63.22.Rc, 61.48.Gh, 78.67.Wj

Moiré patterns correspond to superstructures that occur when two periodic two-dimensional lattices are overlaid at specific angles.¹ In graphene systems, they appear when adjacent graphene layers are misoriented or when the graphene layer is deposited on or covered by another periodic crystalline structure, such as the hexagonal-BN layer. It has been shown recently² that the Moiré pattern interlayer interaction depends strongly on the twist angle between the layers, and the sensitivity of the electronic properties to the twist angle between adjacent layers can be useful in applications such as ultrasensitive strain sensors and ultrathin capacitors,¹ suggesting that systematic studies of misoriented graphene layers are needed. We show in this work that Moiré patterns activate new Raman peaks that can be useful for characterization of misoriented graphene layers.

Raman spectroscopy has proven to be an extremely useful technique to characterize graphene, since it provides information about disorder and defects,³ the atomic structure of graphene edges,⁴ the stacking order between different layers,⁵ the number of graphene layers stacked in a Bernal configuration,⁶ the effect of strain,^{7,8} and charge transfer.^{9–11} Moreover, in resonant Raman investigations, when the energy of the exciting laser can be tuned, we can also obtain further information about the electronic structure and the dispersion of phonons near the Dirac point.^{12,13}

The Raman spectrum of graphene exhibits, other than the first-order G band, a number of specific features associated with phonons within the interior of the graphene Brillouin zone (BZ) that are activated by the selective double-resonance Raman processes, the most important and significant ones being the so-called D , D' and $2D$ (or G') bands.^{3,6,13}

In this Rapid Communication, we report on the observation of families of new Raman peaks that appear in the Raman spectra of misoriented bilayer graphene grown by chemical vapor deposition (CVD) on copper. We ascribe these new peaks to phonon modes within the interior of the graphene Brillouin zone that become Raman active through an umklapp double-resonance (U-DR) Raman process associated with reciprocal lattice vectors of the Moiré pattern supercells.

Graphene films were grown by CVD on a copper-foil enclosure at high temperature (1035 °C). The enclosure was formed by bending copper foil and then crimping the three remaining sides. The graphene grown on the outside of the Cu enclosure showed a high density of bilayers, whereas domains of mostly monolayer graphene were observed on the inside of the Cu enclosure.¹⁴ The Raman measurements were performed in the as-grown sample, using a back scattering configuration at room temperature. Raman maps were obtained in a triple monochromator spectrometer (JY T64000) using the 3.82 eV (325 nm) line of a He-Cd laser as the excitation laser energy. The spot size of the laser was $\sim 1 \mu\text{m}$ using a 40 \times objective, and the laser power was kept below 1 mW. For the resonance Raman experiments, we have used a DILOR XY UV spectrometer and UV microscope (objective 40 \times UV grade A) with a back-illuminated and cooled CCD detector, using the UV lines at 3.40 eV (364.0 nm), 3.53 eV (351.1 nm), 3.69 eV (335.8 nm) and 4.13 eV (300.3 nm) of a 20 W argon laser.

Figure 1(a) shows the Raman spectra obtained in four different regions of the sample, inside and outside the Cu enclosure. The spectrum at the top of Fig. 1(a) was recorded in a region inside the enclosure that contains domains of single-layer graphene (SLG), and shows the D , G , and the $2D$ (or G') bands (the D band appears around 1420 cm^{-1} using the 3.82 eV laser line).^{3,13} The three other spectra in Fig. 1(a) were obtained in three different regions of the film grown on the outside of the Cu enclosure, with a high density of bilayer graphene (BLG) domains. Notice that, in addition to the G band, these three spectra also exhibit a number of sharp extra peaks around 1400 cm^{-1} (the absence of the D band can be ascribed to the high crystalline quality of the sample in these three regions).

Figures 1(b) and 1(c) show the Raman maps of the G band and the extra sharp peak at 1381 cm^{-1} , respectively, obtained in a $30 \times 25 \mu\text{m}^2$ area on the outside of the Cu enclosure. Notice that the extra peak at 1381 cm^{-1} peak appears only in some regions of the probed area, represented by the white parts in the map shown in Fig. 1(c), whereas the G band is observed across

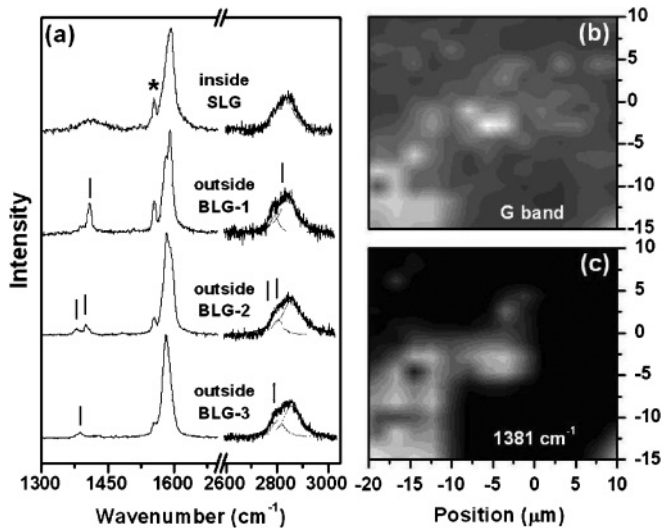


FIG. 1. (a) Raman spectra obtained in four different regions of the sample. The spectrum on the top was recorded inside the Cu enclosure, and the other three were obtained in different regions outside of the Cu enclosure, with bilayer graphene (BLG) domains. The peak marked by an asterisk is an artifact that comes from the substrate. (b) and (c) show Raman maps of the G band and the 1381 cm^{-1} peak, respectively, obtained in a $30 \times 25\ \mu\text{m}^2$ area. In the gray scale, white regions are associated with high-intensity peaks.

the whole area. However, as shown in Fig. 1(b), the intensity of the G band is higher in the regions of the sample where the 1381 cm^{-1} peak appears. Since the G band intensity increases with an increasing number of layers, the maps suggest that the extra peak at 1381 cm^{-1} appears in regions with more than one graphene layer.

The second-order $2D$ (or G') Raman bands are shown in the right side of Fig. 1(a). Notice that the $2D$ band of the SGL sample recorded with the 3.82 eV UV laser line is broader and asymmetric, when compared with the corresponding band recorded with visible photons (we have observed the same behavior for the $2D$ band of exfoliated graphenes). Only slight changes in the position and shape of the $2D$ bands are observed in the BLG spectra. The vertical segments above the $2D$ bands correspond to two times the frequencies of the sharp extra peaks shown in the first-order spectra [left side of Fig. 1(a)], showing that the overtones of these peaks are superimposed with (and also contribute to) the $2D$ bands.

Figure 2(a) shows the Raman spectra in the $1000\text{--}1700\text{ cm}^{-1}$ range, obtained in eight different regions of the graphene films grown on the outside of the Cu enclosure (spots S1 to S8). Notice that a number of Raman sharp extra peaks appear in each spectrum, and their frequencies, shown in Table I, are different in the eight spectra. The average FWHM of these extra peaks is 8 cm^{-1} . It is interesting to note that these peaks are grouped in families of peaks, which always appear in the same spectrum. For example, the maps of the Raman peaks at 1082 , 1400 , and 1473 cm^{-1} (spot S2), presented in Figs. 2(b), 2(c), and 2(d), respectively, show that they appear in the same regions of the sample, with typical dimensions of a several μm .

Figures 3(a), 3(b), and 3(c) show the Raman maps of the peaks at 1381 , 1400 , and 1424 cm^{-1} , which belong to different

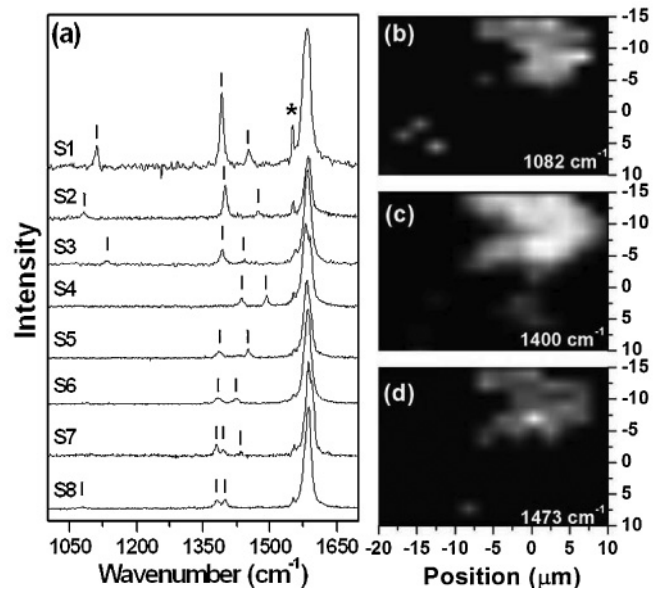


FIG. 2. (a) Raman spectra in the $1000\text{--}1700\text{ cm}^{-1}$ range, obtained in eight different spots in the sample (outside of the Cu enclosure) showing the presence of a number of sharp extra peaks. (b), (c), and (d) show Raman maps of the peaks at 1082 , 1400 , and 1473 cm^{-1} , respectively, which appear in spectrum S2 of (a).

families of peaks and are observed, respectively, in spectra S8, S2, and S6 of Fig. 2(a). Notice that each peak appears in distinct and complementary regions of the sample, evidencing the presence of domains with dimensions of several μm . This result rules out the assignment of these extra peaks as due to topological defects in graphene,¹⁵ or to molecules deposited on the graphene layer.

Gupta *et al.*¹⁶ also observed the presence of a new Raman peak in a mechanically exfoliated graphene folded upon itself, and interpreted this new peak as due to a finite-wave vector associated with the interlayer perturbation that gives rise to a double-resonant Raman process in graphene. The observation of extra peaks, which was not reported in previous Raman studies of twisted bilayer graphenes,^{17,18} was recently also observed in a Raman study of rotationally stacked bilayer graphene obtained by mechanical exfoliation.¹⁹

In our theoretical interpretation of the new Raman peaks in Figs. 1 and 2, we consider a periodical perturbation ΔV to graphene originated from the twisted-double-layer Moiré

TABLE I. Frequencies (in cm^{-1}) of the extra Raman peaks observed in spectra shown in Fig. 2(a), obtained in different spots of the sample. The frequencies of the G band are not shown.

Spots	LA	TO	LO		
S1	1110	1391	1452	1588	
S2	1082	1400	1473	1589	
S3	1134	1392	1443	1591	
S4			1436	1492	1591
S5		1386		1452	1592
S6		1383	1424		1588
S7		1379	1395	1434	1595
S8	1078	1381	1399		1588

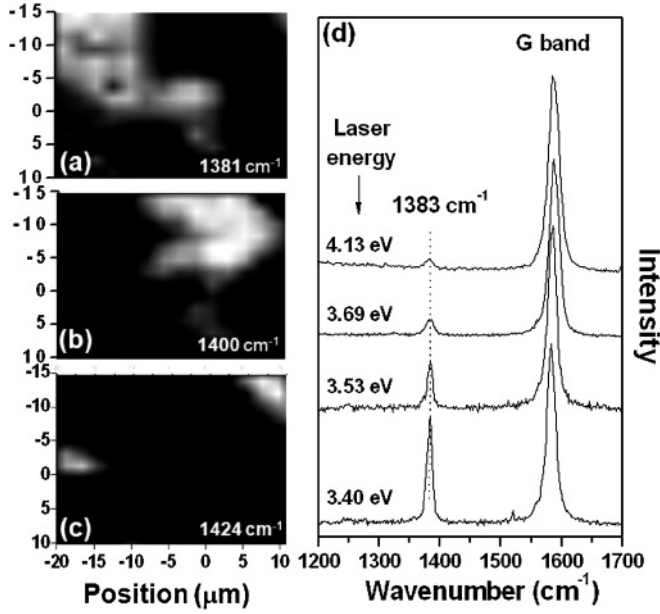


FIG. 3. Raman maps of the peaks at (a) 1381, (b) 1400, and (c) 1424 cm^{-1} , recorded in a $25 \times 25 \mu\text{m}^2$ area of the sample. (d) Raman spectra taken in the same spot of the sample, showing the extra peak at 1383 cm^{-1} recorded with four different laser energies.

pattern. The perturbation allows for elastic scattering from electron states $\psi(\mathbf{k})$ to $\psi(\mathbf{k}')$, described by matrix elements $M_{\mathbf{k}\mathbf{k}'} = \langle \psi(\mathbf{k}') | \Delta V | \psi(\mathbf{k}) \rangle$. This leads to a double-resonance (DR) Raman scattering process similar to those of the D and D' bands, where the electron is (i) optically excited, (ii) inelastically scattered by a phonon of wave vector \mathbf{q} , (iii) back-scattered by the elastic scattering process with wave vector $-\mathbf{q}$, and (iv) radiatively de-excited. In the cases of the D and D' bands, the local perturbation ΔV , which is due to defects, leads to non-null values of $M_{\mathbf{k}\mathbf{k}'}$ in a continuum range of $\mathbf{q} = \mathbf{k} - \mathbf{k}'$.³ In contrast, the periodic Moiré perturbation ΔV leads to allowed scattering (non-null $M_{\mathbf{k}\mathbf{k}'}$) only for a discrete set of $\mathbf{k}' - \mathbf{k} = \mathbf{G}$, where \mathbf{G} is the set of the reciprocal lattice vectors of the Moiré pattern. This process can therefore be described as an umklapp DR process for the Moiré lattice. From momentum conservation we have $\mathbf{q} = \mathbf{G}$, and therefore the only relevant phonon scattering events in such umklapp-Moiré DR process are those for phonons with wave vectors \mathbf{G} . This is schematically shown in Fig. 4. Figure 4(a) shows the exact Moiré pattern generated by two layers of graphene rotated by a given angle with respect to each other (9.43° in this case) and, in Fig. 4(b), each point within the interior of the Brillouin zone (BZ) of graphene corresponds to an allowed wave vector \mathbf{G} of the reciprocal lattice of the superstructure shown in Fig. 4(a). The DR Raman process involving one phonon with a wave vector that matches a reciprocal lattice vector of the Moiré superlattice is also represented in Fig. 4(b), for both the intervalley and intravalley DR processes.

The similarity between the physical processes (elastic scattering, double resonance) involved in the D band and those of the umklapp-Moiré peaks suggests that they should occur at similar spectral ranges, for a given laser photon energy. This is shown in Fig. 1(a), where we present the Raman spectra of monolayer graphene in a region of the sample with defects,

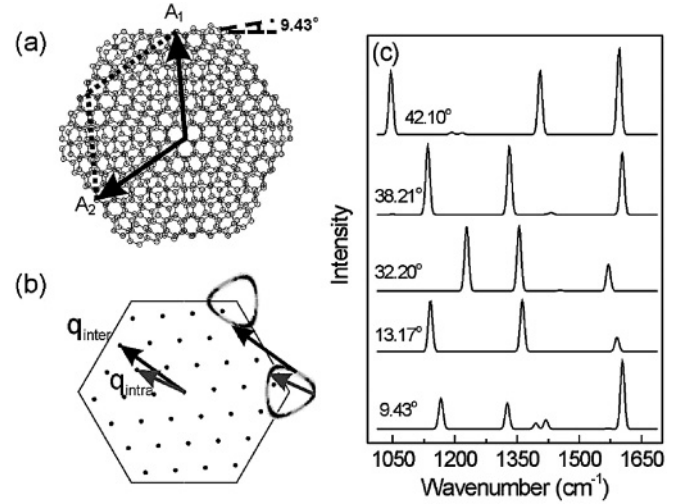


FIG. 4. (a) Moiré pattern in two twisted graphene layers. (b) Wave vectors of the Moiré pattern superlattice and two possible DR Raman processes (intervalley and intravalley). (c) Simulated Raman spectra using Eq. (1) with sets of \mathbf{G}_B vectors for several possible twist angles between graphene layers. The G band is not shown.

where the broad D band can be observed centered around 1420 cm^{-1} . Notice that the frequencies of a number of sharp peaks of the umklapp-Moiré spectra of Figs. 1(a) and 2(a) are overlaps with the broader D band shown at the top of Fig. 1(a). The main difference is that umklapp-Moiré peaks are much narrower than the D band, and they are not dispersive. This is shown in Fig. 3(d), which depicts the Raman spectra taken in the same spot of the sample but recorded with four different laser energies (3.40, 3.53, 3.69 and 4.13 eV). Notice that the position of the peak at 1383 cm^{-1} does not depend on the laser energy, but only its intensity changes, as expected for an umklapp double resonance (U-DR) process. In this type of process, each phonon with allowed wave vector \mathbf{G} will achieve resonance at a specific laser energy. Notice, from Fig. 3(d), that the resonance condition for the peak at 1383 cm^{-1} has not yet been achieved at 3.40 eV, and it should occur at lower laser energies.

We simulated the U-DR Raman spectrum of the Moiré pattern, $I(\omega, E_{\text{laser}})$, as

$$I(\omega, E_{\text{laser}}) = \sum_{\mathbf{G}, s} f(\mathbf{G}, s, E_{\text{laser}}) \delta(\omega - \omega_{\mathbf{G}, s}) \quad (1)$$

where $\omega_{\mathbf{G}, s}$ is the graphene phonon frequency at \mathbf{G} for branch s and $f(\mathbf{q}, s, E_{\text{laser}})$ is the intensity for the DR Raman scattering involving a phonon mode of branch s with wave vector \mathbf{q} . The phonon dispersions are obtained from *ab initio* density functional theory calculations with many-body corrections as in Refs. 20,21. We only consider here the longitudinal acoustic (LA), transverse optic (TO) and longitudinal optic (LO) branches. For the intervalley double-resonant processes, we consider the LA and the TO branches, which are allowed by symmetry.¹³ For such processes, involving a photon energy E_{laser} , maximum scattering intensity occurs for phonon wave vectors near a specific one, $\mathbf{q}_{\text{inter}}(E_{\text{laser}})$, which is the minimum-modulus wave vector that connects the electronic band valley near \mathbf{K} with energy $E_{\text{laser}}/2$ to the valley near \mathbf{K}' with energy $E_{\text{laser}}/2 - \hbar\omega(\mathbf{q})$. As an

approximation, we neglect the phonon energy term in the last expression and obtain $\mathbf{q}_{\text{inter}} = \alpha(E_{\text{laser}})(\mathbf{q}_K - \mathbf{q}_{K'})$, where $\alpha(E_{\text{laser}})$ is obtained from calculated quasiparticle bands.²² We consider a phenomenological expression for the intervalley f as $f_{\text{inter}}(\mathbf{q}, s, E_{\text{laser}}) = A(E_{\text{laser}})e^{-[\mathbf{q} - \mathbf{q}_{\text{inter}}(E_{\text{laser}})]^2 / \Delta q}$, with $\Delta q = 0.1q_{\text{inter}}$. The prefactor $A(E_{\text{laser}})$ is proportional to the square of the elastic scattering matrix between the two electronic states. Although this quantity is not known, calculations for twisted double layers^{23,24} indicate that it would only be significant above $E_{\text{laser}} \approx 2.5$ eV. This is consistent with the absence of Moiré peaks with E_{laser} in the visible range. The LO branch appears only for intravalley double-resonant processes.¹³ In this case, maximum scattering intensity occurs at the phonon wave vectors with modulus q_{intra} . Accordingly, we consider a phenomenological expression for the intervalley f as $f_{\text{intra}}(q, s, E_{\text{laser}}) = (1/2)B(E_{\text{laser}})e^{-(q - q_{\text{intra}})^2 / \Delta q}$, with $q_{\text{intra}} = |\mathbf{q}_K - \mathbf{q}_{K'}| - q_{\text{inter}}$.

We computed the spectra, using Eq. (1), with sets of \mathbf{G} vectors corresponding to several possible twist angles between graphene layers, and the results are shown in Fig. 4(c). Notice that, for all angles, the simulated Raman peaks group at three distinct wave-number regions. The first and second groups, respectively, in the ranges 1050–1250 and 1325–1450 cm^{-1} , show stronger dispersions with respect to twist angles, and come from the LA and TO branches, respectively. The third group, near 1600 cm^{-1} and associated with the LO phonon branch, is almost dispersionless with respect to twist angle. These three groups in the simulated spectrum would correspond to the experimentally observed ones shown in Fig. 2(a) and in Table I in the ranges 1070–1140, 1380–1490, and 1590–1600 cm^{-1} , respectively.

Although the above interpretation is strictly valid only for exact Moiré patterns, it can also be considered as an approximate theory for incommensurate patterns, in the sense that we can find graphene's translation vectors that best match the primitive lattice vectors \mathbf{A}_1 and \mathbf{A}_2 and perform the calculations for such lattice. It is also important to emphasize that the positions of the simulated extra peaks depend on the phonon dispersion approximation, and the agreement between the simulated and observed spectra is only qualitative. Moreover, the intensities of the simulated Raman bands are not the same as the observed ones, since we have not taken into account the selection rules and the matrix elements for the calculation of these bands. Anyway, the qualitative agreement between the observed and simulated spectra shown in Figs. 2(a) and 4(c) further supports our interpretation of families of Raman peaks associated with Moiré patterns of graphene layers twisted with different angles. In a sample of two graphene layers presenting domains misoriented between each other, the maps of the Moiré peaks can give a direct image of these domains.

An important extension of this work will be the measurement of the Moiré pattern Raman modes in BLG samples for which the twist angles have been previously measured by TEM. The precise association of the Raman positions with the twist angle will provide precise data for an accurate determination of the phonon dispersion within the interior of the BZ of graphene.

This work was supported by the Instituto Nacional de Ciencia e Tecnologia (INCT) em Nanomateriais de Carbono - MCT, CNPq, and FAPEMIG (Brazil).

¹A. H. MacDonald and R. Bistritzer, *Nature* **474**, 453 (2011).

²A. Luican, G. Li, A. Reina, J. Kong, R. R. Nair, K. S. Novoselov, A. K. Geim, and E. Y. Andrei, *Phys. Rev. Lett.* **106**, 126802 (2011).

³M. A. Pimenta, G. Dresselhaus, M. S. Dresselhaus, L. G. Cancado, A. Jorio and, R. Saito, *Phys. Chem. Chem. Phys.* **9**, 1276 (2007).

⁴L. G. Cancado, M. A. Pimenta, B. R. A. Neves, M. S. S. Dantas, and A. Jorio, *Phys. Rev. Lett.* **93**, 247401 (2004).

⁵L. G. Cancado, K. Takai, T. Enoki, M. Endo, Y. A. Kim, H. Mizusaki, N. L. Speziali, A. Jorio, and M. A. Pimenta, *Carbon* **46**, 272 (2008).

⁶A. C. Ferrari, J. C. Meyer, V. Scardaci, C. Casiraghi, M. Lazzeri, F. Mauri, S. Piscanec, D. Jiang, K. S. Novoselov, S. Roth, and A. K. Geim, *Phys. Rev. Lett.* **97**, 187401 (2006).

⁷T. M. G. Mohiuddin, A. Lombardo, R. R. Nair, A. Bonetti, G. Savini, R. Jalil, N. Bonini, D. M. Basko, C. Galiotis, N. Marzari, K. S. Novoselov, A. K. Geim, and A. C. Ferrari, *Phys. Rev. B* **79**, 205433 (2009).

⁸M. Y. Huang, H. G. Yan, C. Y. Chen, D. H. Song, T. F. Heinz, and J. Hone, *Proc. Natl. Acad. Sci. USA* **106**, 7304 (2009).

⁹S. Pisana, M. Lazzeri, C. Casiraghi, K. S. Novoselov, A. K. Geim, A. C. Ferrari, and F. Mauri, *Nat. Mater.* **6**, 198 (2007).

¹⁰J. Yan, Y. Zhang, P. Kim, and A. Pinczuk, *Phys. Rev. Lett.* **98**, 166802 (2007).

¹¹A. Das, S. Pisana, B. Chakraborty, S. Piscanec, S. K. Saha, U. V. Waghmare, K. S. Novoselov, H. R. Krishnamurthy, A. K. Geim, A. C. Ferrari, and A. K. Sood, *Nat. Nanotech.* **3**, 210 (2008).

¹²L. M. Malard, J. Nilsson, D. C. Elias, J. C. Brant, F. Plentz, E. S. Alves, A. H. Castro Neto, and M. A. Pimenta, *Phys. Rev. B* **76**, 201401 (2007).

¹³L. M. Malard, M. A. Pimenta, G. Dresselhaus, and M. S. Dresselhaus, *Phys. Rep.* **473**, 51 (2009).

¹⁴X. Li, C. W. Magnuson, A. Venugopal, R. M. Tromp, J. B. Hannon, E. M. Vogel, L. Colombo, and R. S. Rouff, *J. Am. Chem. Soc.* **133**, 2816 (2010).

¹⁵V. N. Popov, L. Henrard, and P. Lambin, *Carbon* **47**, 2448 (2009).

¹⁶A. K. Gupta, Y. Tang, V. H. Crespi, and P. C. Eklund, *Phys. Rev. B* **82**, 241406 (2010).

¹⁷P. Poncharal, A. Ayari, T. Michel, and J.-L. Sauvajol, *Phys. Rev. B* **78**, 113407 (2008).

¹⁸A. W. Robertson and J. H. Warner, *Nano Lett.* **11**, 1182 (2011)

¹⁹V. Carozo, C. M. Almeida, E. H. M. Ferreira, L. G. Cancado, C. A. Achete, and A. Jorio, *Nano Lett.* **11**, 4527 (2011).

²⁰M. Lazzeri, C. Attacalite, L. Wirtz, and F. Mauri, *Phys. Rev. B* **78**, 081406 (2008).

²¹P. Venezuela, M. Lazzeri, and F. Mauri, *Phys. Rev. B* **84**, 035433 (2011).

²²P. E. Trevisanutto, C. Giorgetti, L. Reining, M. Ladisa, and V. Olevano, *Phys. Rev. Lett.* **101**, 226405 (2008).

²³Z. Ni, L. Liu, Y. Wang, Z. Zheng, L. J. Li, T. Yu, and Z. Shen, *Phys. Rev. B* **80**, 125404 (2009).

²⁴S. Latil, V. Meunier, and L. Henrard, *Phys. Rev. B* **76**, 201402(R) (2007).